Nuclear Science and Techniques (2024) 35:172
https://doi.org/10.1007/s41365-024-01522-1

Design of a large momentum acceptance proton therapy gantry utilizing AG-CCT magnets

Yi-Cheng Liao[1] · Xu Liu[1] · Wei Wang[1] · Zi-Yi Yang[1] · Qu-Shan Chen[1] · Bin Qin[1]

Received: 9 October 2023 / Revised: 4 February 2024 / Accepted: 19 February 2024 / Published online: 21 September 2024

Abstract

The application of superconducting (SC) technology enables magnets to excite strong fields with small footprints, which has great potential for miniaturizing proton therapy gantries. However, the slow ramping rate of SC magnets results in a low treatment efficiency compared with normal-conducting (NC) gantries. To address this problem, this study proposes a compact proton therapy gantry design with a large momentum acceptance utilizing alternating-gradient canted-cosine-theta (AG-CCT) SC magnets. In our design, a high-transmission degrader is mounted in the middle of the gantry, and the upstream beamline employs NC magnets with small apertures. Downstream of the degrader, large-bore AG-CCT magnets with strong alternating focusing gradients are set symmetrically as a local achromat, which realizes a momentum acceptance of 20% (or 40% in the energy domain). Therefore, only three magnetic working points are required to cover a treatment energy of 70–230 MeV. Owing to the large momentum acceptance, the proton beam after the degrader can be directly delivered to the isocenter without truncating its energy spectrum, which can significantly increase the treatment efficiency but causes severe dispersion effects during pencil beam scanning. Therefore, a compensation method was introduced by tuning the normal and skewed quadrupoles during the scanning process. As a result, the new gantry not only presents a remarkable reduction in the size and weight of the facility but also shows good potential for fast treatment.

Keywords Alternating-gradient canted-cosine-theta magnets · Large momentum acceptance gantry · Pencil beam scanning · Proton therapy

1 Introduction

Proton therapy facilities require proton beam delivery with the highest nominal energy of 230–250 MeV, which consequently requires large bending radii and heavy iron yokes for normal-conducting (NC) magnets to guide the beam along the orbit. The gantry component, which is the final part of the proton therapy beamline, mainly consists of NC magnets. It bends and transports the proton beams to the target volume with an irradiation angle between ± 180°. Most gantries are cumbersome, with lengths exceeding 10 m and weights exceeding 100 t [1, 2]. However, with the popularization and maturation of proton therapy technology, more compact facilities with smaller footprints and lighter weights are needed for patients and hospitals, considering economics and convenience. Adopting superconducting (SC) magnets is a promising alternative for miniaturizing gantries because they can excite stronger magnetic fields without iron yokes. However, the main drawback of this method is its slow ramping rate. Momentum modulation is performed in steps of $\Delta p/p = 1\%$–2% with a ramping time of 0.1–2 s per step [3]. Therefore, it is necessary to design an SC gantry with a large momentum acceptance (LMA) so that the magnetic field can remain constant while delivering proton beams within a wide energy range.

The main task in designing an LMA gantry is to suppress the dispersion effect at both the maximum dispersion point and the isocenter. Therefore, effective achromatic

This work was supported by the National Natural Science Foundation of China (No.11975107, 12205111).

✉ Xu Liu
lxhustliu@hust.edu.cn

✉ Bin Qin
bin.qin@mail.hust.edu.cn

[1] State Key Laboratory of Advanced Electromagnetic Technology, Huazhong University of Science and Technology, Wuhan 430074, China

sections should be designed with high-order beam optics to suppress the dispersion below that in conventional NC gantries. ProNova SC360 was the first commercial facility equipped with an SC gantry [4, 5]. The gantry consists of two SC local achromatic bending sections and realizes a momentum acceptance of $\Delta p/p \geq 6\%$, which is six times higher than that of conventional NC gantries. The LMA gantry designed by Lawrence Berkeley National Laboratory (LBNL) also adopted a fully SC bending design [6]. An alternating-gradient canted-cosine-theta (AG-CCT) magnet has been introduced that provides strong alternating focusing forces and acts as an independent local achromatic bending section [7]. This gantry was composed of three AG-CCT magnets and several NC combined-function magnets. The gantry achieved a momentum acceptance of $\Delta p/p \approx 25\%$, with which it was possible for the gantry to cover the full energy range of 70–230 MeV with only three magnetic working points.

A full SC design with local achromaticity often requires a strict lattice optimization process because residual dispersion accumulates and is transported to the next SC section. This problem can be solved by setting collimators at the ends of the SC sections or by adding quadrupoles between them to tune the beam spots. However, this results in beam losses or larger gantry footprints. A hybrid SC design is another gantry option used in cyclotron-based facilities [8, 9].

For compactness, an energy degrader is placed in the middle of the gantry. In this way, achromatic design should only be applied to the downstream section, which greatly increases the ease of design. The upstream section can be either SC or NC design. Owing to the quasi-monoenergetic and low-emittance characteristics of the beam extracted from the cyclotron, the upstream beamline can use small-aperture magnets without a strict achromatic design. In addition to the gantry designs discussed above, novel concepts such as gantries with fixed-field superferric magnets [10] and non-rotating gantries [11–13] have also been studied in recent years.

In this study, a physical design of an SC LMA gantry based on AG-CCT magnets is proposed. The design is based on our previous work [14–16] and adopts a hybrid SC design pattern. Compared to our previous studies, we expanded the momentum acceptance and presented a more detailed component design considering the operational situation during treatment.

The remainder of this paper is organized as follows. First, we provide an overview of the designed LMA gantry structure, key parameters of the gantry, and information about the degrader component in Sect. 2. The design of the beam optics for the SC bending section is presented in Sect. 3, including the beam envelope, momentum acceptance value, and beam spot properties at the isocenter. In Sect. 4 we propose a compensation method for the scanning dispersion, which is mainly caused by the abandoning of the energy selection slit during pencil beam treatment. The potential of LMA beams is discussed in Sect. 5. Finally, the conclusions and outlook are presented in Sect. 6.

2 Structure of the LMA gantry

2.1 An overview of the LMA gantry

The proposed LMA gantry is intended for applications in cyclotron-based proton therapy systems; therefore, a degrader component is essential for beam energy modulation. In the proposed design, the degrader is placed in the middle of the gantry, as shown in Fig. 1, and divides the gantry into 2 sections: the NC and SC sections. The NC section delivers a fixed-energy proton beam from the cyclotron to the degrader. No strict achromatic design is required in this section because the particle–matter interaction at the downstream degrader is the deciding factor in the beam shape. It contains a 1.4 m bending-radius NC dipole with an air gap of 30 mm and three 50 mm aperture NC quadrupoles (NCQ1–3). Owing to the low-emittance beam extracted from the cyclotron, the magnetic apertures in the NC section are nearly half of those in a conventional NC gantry.

Downstream of the degrader, the SC section is a vital component for realizing LMA and comprises two 67.5° AG-CCT magnets with a small bending radius of 0.95 m, two NC quadrupoles (NCQ4 and 5), a coil-type quadrupole (NCQC), and an NC skewed quadrupole (NCQS).

The AG-CCT magnets shown in Fig. 1, are formed by four layers of SC coils. The two outer layers provide bending forces and the two inner layers have three curved segments with alternating gradients (F-D-F). Their magnetic fields are mirror-symmetrically set about the quadrupoles for achromaticity.

The space downstream of the SC section is limited owing to the compactness of the gantry. Therefore, the NCQC magnet was designed as a coil-type magnet such that it could be placed close to AG-CCT2. A discrete cosine-theta (DCT) or conventional cosine-theta (CT) magnet may be used. The fringe field overlap will be evaluated later on in the magnet design phase.

After the NCQC, a compact nozzle component lies in the last part of the gantry. It paints the planning target volume by switching the strength of the scanning magnet in both transverse planes. The nozzle consists of a combined-function scanning magnet (CFSM), which provides a bending force simultaneously in both transverse planes, a helium chamber, and several ionization chambers. The nozzle is expected to cover a scanning field of 25 cm × 25 cm. The source-to-axis distance (SAD) is set to 1.5 m according to a clinical

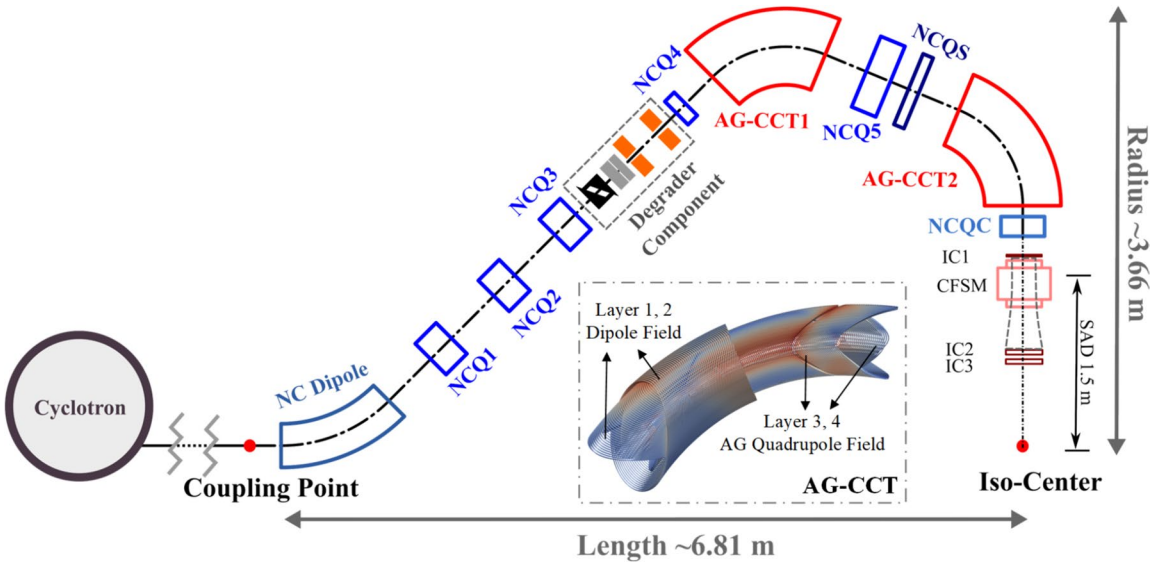

Fig. 1 (Color online) Schematic of the proposed LMA gantry. The coil layers of the curved 67.5° AG-CCT magnet are presented in the inset, in which half of the two outer dipole layers have been removed to show the AG quadrupole layers inside

Table 1 Key parameters of the LMA gantry

	Parameters	Values
Gantry	Length (m)	6.81
	Height[a] (m)	3.66
	Scanning field (cm^2)	25×25
	SAD (m)	1.50
NC dipole	Bending radii (m)	1.40
	Bending angle (°)	45.00
	Air gap (mm)	30.00
AG-CCT	Bending radii (m)	0.95
	Bending angle (°)	67.50
	Inner bore radius (m)	0.12
	Radius of good field region (m)	0.09
	Maximum gradient (T/m)	15
	Coil layers	4

[a]Note that the height of the gantry does not include peripheral mechanical support structures

Table 2 Properties of the NC quadrupoles

	Bore diameter (mm)	Effective length (mm)	Maximum gradient (T/m)
NCQ1–3	50	180	24
NCQ4	60	120	18
NCQ5	240	180	6
NCQS	240	100	3
NCQC	120	180	6

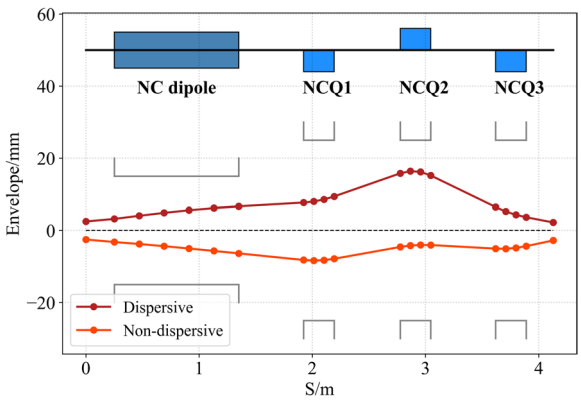

Fig. 2 (Color online) Envelope results for the NC section. (The line above the horizontal axis represents the envelope result in the dispersive direction and the line below the horizontal axis represents the envelope in the non-dispersive direction)

study [17]. The key gantry parameters are listed in Tables 1 and 2 lists the properties of the NC quadrupoles.

2.2 High transmission degrader component

The optical design of the NC section primarily seeks to form a small and focused beam spot at the entrance of the degrader to reduce beam loss. Figure 2 illustrates the envelope (2σ) of the NC section.

Beam optics simulations were conducted on COSY-Infinity [18], with the linear-optics effect included. The initial beam energy from the cyclotron was 240 MeV with an energy spread $dE/E = \pm 0.116\%$ (1σ) [19]. The beam emittance at the NC section is 8π mm · mrad (2σ), which is moderate for most cyclotrons but is much smaller than that of the

degraded beam. Consequently, resistive magnets with small apertures are employed to further reduce the gantry weight.

Subsequently, the proton beams are transported to the degrader, where the beam energy can be modulated to the expected value corresponding to the treatment plan by changing the stopping length of the degrader. According to our previous multiwedge degrader design for the HUST-PTF [20], the Coulomb scattering occurring in the high-density graphite wedge drastically increases the beam emittance such that most of the protons are blocked by the downstream collimators. To suppress the growth of the beam emittance and increase the transmission efficiency of the degrader component, low-atomic-number materials should be used for energy modulation. Figure 3 shows the new degrader design, which is based on Ref. [21]. It consists of a hybrid degrader set and copper collimator set. The degrader set contains a pair of high-density graphite wedges and two B_4C blocks. The energy modulation range of 70–230 MeV can be divided into three parts, as listed in Table 3. There are some overlaps in the energy range when the B_4C blocks switch. However, here we discuss only the energy range used in treatment. It should be noted that switching of the B_4C blocks should be avoided during treatment because their slower movement may last approximately one second. According to our degrader design, the high-energy range covers the deposition range of 11.7 cm, within which approximately 60% of the clinical treatment can be conducted with no or only one B_4C switch [22].

Two copper collimators are installed downstream of the degrader set to restrict the degraded beam size and divergence. The beam shape at 70 MeV was simulated and used as the initial beam shape at the entrance of the SC section with an emittance of approximately 40π mm · mrad (2σ).

To evaluate the beam properties after energy modulation, a Monte Carlo simulation was performed on Geant-4 [23] using the initial beam parameters from the exit of the NC section. The result of the HUST-PTF multiwedge degrader design was set as a benchmark. Figure 4 presents the beam properties along the nominal beam energy at the exit of the degrader set. As the energy of the proton beam decreases from 230 to 70 MeV, the beam emittance of the hybrid

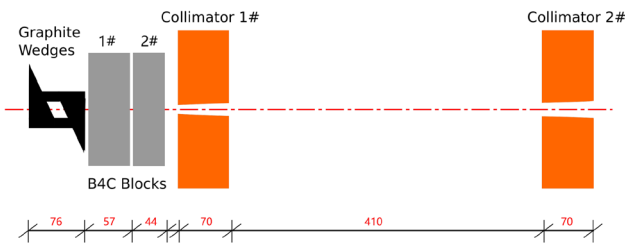

Fig. 3 (Color online) Layout of the hybrid degrader component in the LMA gantry. Unit: mm

Table 3 The energy modulation plan of the degrader

	Energy range (MeV)	Modulation movement
Low	70–120	Graphite wedges + B_4C block 1 and 2
Middle	120–180	Graphite wedges + B_4C block 1
High	180–230	Graphite wedges

degrader set increases but is smaller than that of the multiwedge design. It reaches a maximum beam emittance of 115.7π mm · mrad (1σ) at 70 MeV, which is approximately 75% that of the multiwedge degrader. The energy spread of the degraded beam is similar for the two degrader designs, and the maximum energy spread is ±5.2% at 70 MeV.

Finally, the transmission efficiency of the degrader was evaluated, which is a key metric of the facility and strongly affects the beam intensity at the isocenter. Figure 5 displays the transmission efficiency as a function of the beam energy. The transmission of the hybrid degrader is similar to that of the multi-wedge design in the high-energy range but approximately 50% higher in the low-energy range. Thus, the hybrid degrader design is proven to improve the beam intensity of the gantry.

3 Beam optics design in the SC section

The AG-CCT magnets in the SC section have three curved segments with strong alternating gradients (F-D-F) and are set mirror-symmetrically for achromaticity. This concept originates from a typical double-bend achromat (DBA) lattice. However, unlike the completely symmetrical setting in a linear optics system, the even-order effects of the high-order

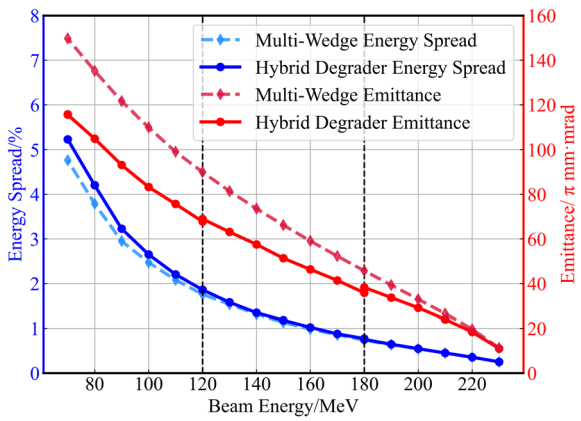

Fig. 4 (Color online) Comparison of beam properties as functions of beam energy at the entrance of the collimator for the hybrid and multi-wedge degraders. (Blue lines represent the energy spread of the beam and red lines represent the beam emittance [1σ]. Both lines for the hybrid degrader are divided into three parts corresponding to the energy modulation plan.)

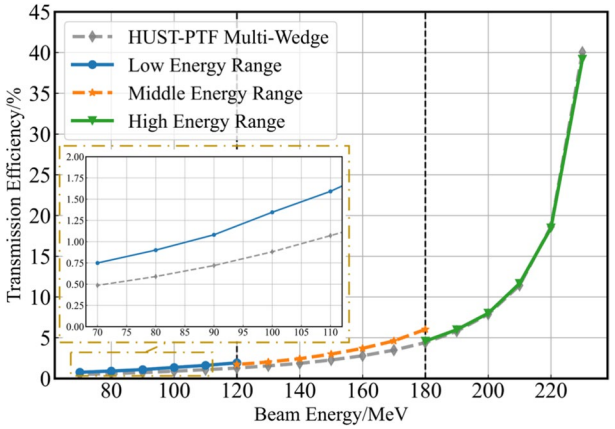

Fig. 5 (Color online) Comparison of the transmission efficiency as a function of beam energy for the hybrid degrader and the HUST-PTF degrader

Table 4 Constraints of the proton beam within the whole momentum acceptance range. (The beam sizes in the table refer to 1σ values.)

Description	Limitation
Beam spot center deviation (mm)	< 1.5 [a]
Beam spot size fluctuation (mm)	< 1.0
Beam spot ellipticity	$< 10\,\%$
Maximum beam size (mm)	< 6.0
Minimum beam size (mm)	> 1.5
Maximum beam envelope (mm)	< 90.0

[a]Note that the center deviation can be corrected by the scanning magnets during treatment

achromat design cause a slightly asymmetrical beam distribution. Therefore, in the optics matching phase, we maintain a symmetrically set magnetic field in the SC section because of design simplicity and manufacturing costs, but leave the drift length tunable. A weak sextupole component was added to the 2nd segment of the AG-CCT to help suppress the high-order dispersion effect by changing the winding path of the coil.

High-order beam optics effects of up to the 5th order are included in the design of the SC section in COSY, owing to its relatively wide range of momentum acceptance. Sharp cutoff fringe field (SCOFF) model magnets were adopted for an efficient simulation. Therefore, the lattice of the SC section should be adjusted according to a realistic field distribution later on when the design of AG-CCT magnets is accomplished. Notably, in high-order optics, the lattice-matching process cannot be performed by optimizing the transfer map elements. The direct control of the beam shape with a high-order effect is a more practical approach. In addition, the beam spot size cannot be characterized by a few representative particles because it's not a laminar beam. Therefore, multiparticle tracking (5000 particles in this case) is the most reliable way to characterize the true beam spot properties, albeit very time-consuming.

The initial beam parameters of the SC section are determined by the collimator design in Sect. 2.2, and the beam spot at the isocenter should meet the constraints in Table 4 within the whole momentum acceptance range in accordance with clinical requests [24–27]. The beam spot ellipticity is defined as:

$$\varepsilon = \frac{2\left|\sigma_x - \sigma_y\right|}{\sigma_x + \sigma_y}. \tag{1}$$

Lattice optimization is performed based on the search algorithm NSGA-III [28]. The constraints of the beam spots are quantified as optimization targets in the algorithm. A detailed optimization procedure for the SC section can be found in [15].

The size and ellipticity of the beam spot at the isocenter after optimization are shown in Fig. 6 as functions of momentum offset. The results suggest that the gantry achieves a momentum range of approximately −9.5 to 10.5% under the beam constraints listed in Table 4. Figure 7 shows the envelope results of the SC section at momentum offsets of −9.5%, 0%, and 10.5%. The beams pass through the large-bore AG-CCT magnets within the good-field region (GFR) of 90 mm radius and form consistent round beam spots at the isocenter. Although the GFR of the AG-CCT is defined as 3/4 of the inner bore, it should be carefully considered at both ends of the magnet. Because the boxes corresponding to the magnets in Fig. 7 only represent the optical boundaries (or effective length), there is still longitudinal space occupied by the straight, extended spars. In this case, the maximum envelope is limited to 78 mm at the ends of the AG-CCT magnet, or the particles will be lost. In summary, the particle-tracking results for the SC section prove that the designed LMA gantry achieves a wide momentum acceptance of $\Delta p/p = 20\%$.

With such large momentum acceptance, there is no need to truncate the energy spectrum of the beam after energy modulation using an energy-selection slit as conventional facilities do. This can significantly reduce the beam loss and increase the beam intensity. The energy spread of the proton beam may increase from the conventional figure of ±0.5% to the full spread of ±5.2% while it is still under the acceptance of the gantry. In Ref. [29] we proved that the intensity of a beam with an untruncated energy spectrum (untruncated beam) is four times higher than a truncated beam in the low energy range. Therefore, the treatment

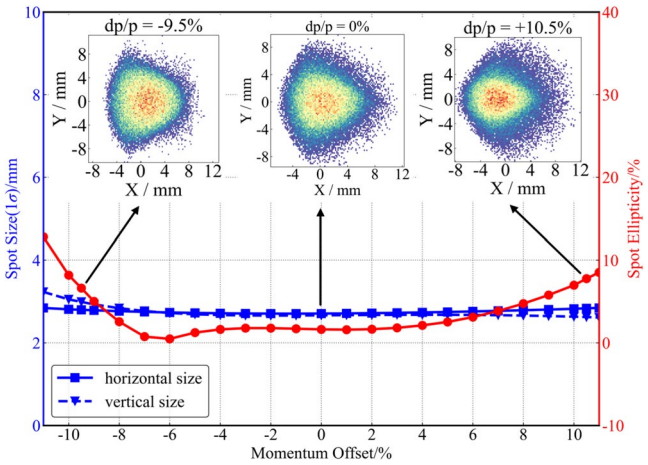

Fig. 6 (Color online) Beam spot size at the isocenter as a function of momentum offset. The three insets are beam heatmaps with momentum offsets of −9.5%(left), 0%(middle), and +10.5%(right) at the isocenter

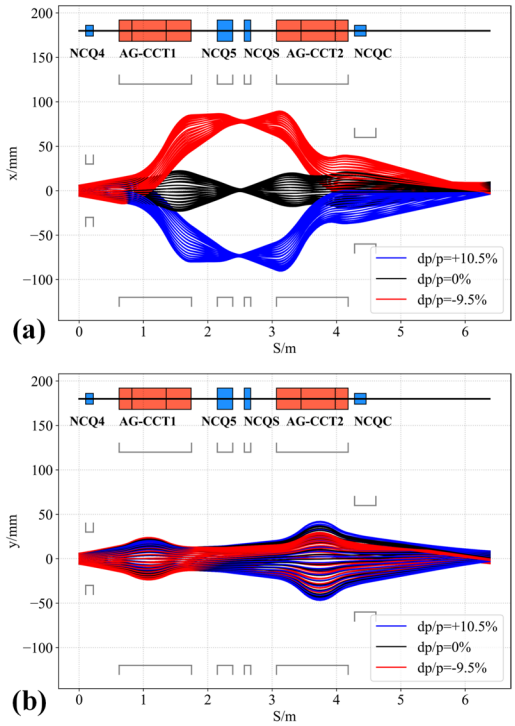

Fig. 7 (Color online) Envelope results for the SC section including 5th order beam optics. **a** Result in the dispersive direction. **b** Result in the non-dispersive direction. (The red, black, and blue lines represent the trajectories of particles at momentum offsets of −9.5%, 0%, and +10.5%, respectively.)

time can be remarkably reduced, which also helps improve the comfort of the treatment experience for patients.

4 Compensation of the scanning dispersion

The untruncated beam can boost the dose rate by a maximum of four times compared to conventional facilities at 70 MeV. This also increases the energy spread of the beam in the low-energy range, which results in an extra dispersion effect during pencil beam scanning. Therefore, the bending force of the CFSM magnet causes an increase in the beam spot size in the dispersive direction when the proton beam travels through the scanning magnet. Furthermore, the dispersive plane rotates with the bending force. Thus, the round beam spot turns into a tilted oval as the beam spot scans away from the center of the scanning field. The length of the major axis of the oval is approximately proportional to the distance between the beam and scanning field centers. This phenomenon is rarely discussed in other studies because the energy spread of most current proton therapy facilities is approximately ±0.5%. Therefore, their dispersion effect is nearly an order of magnitude lower than that observed in our study. To overcome this, a new constraint was introduced to characterize the tilt of the beam spot.

$$\tau = \left| \frac{\sigma_{13}}{\sqrt{\sigma_{11} \cdot \sigma_{33}}} \right| = \left| \frac{\mathrm{Cov}(x, y)}{\sqrt{\mathrm{Var}[x] \cdot \mathrm{Var}[y]}} \right|. \quad (2)$$

τ is the correlation coefficient between the x- and y-distributions of the beam spot. The value of τ should be limited to less than 0.15 as a quasi-round beam spot.

Clearly, the rotating dispersion effect cannot be eliminated or suppressed because it is impractical to add an additional achromatic section downstream of the CFSM. Therefore, an optional solution is to reduce the beam size in advance to compensate for the growth caused by the dispersion. Naturally, the NC magnets in the SC section should be adjustable as compensation knobs during pencil

beam scanning. By re-matching all NC quadrupoles in the SC section as the scanning point switches, the beam spot at the isocenter meets the clinical requirements while the AG-CCT field is fixed. To achieve this, the ramping speed of the NC quadrupoles should be equivalent to that of CFSM. Note that at least one skewed NC quadrupole (NCQS), as a key element in the compensation method, should be added to the SC section because of its rotating dispersive direction. The optical simulation results suggest that the skewed quadrupole NCQS works best between two bending AG-CCT magnets. Because of the large bores and fast ramping requirements, the NC quadrupoles in the SC section should be maintained at a low field strength. Detailed designs of fast-ramping quadrupoles and their compensation control systems will be performed in a future study.

Although the transverse phase spaces of the proton beam are coupled owing to the NCQS, they do not affect the treatment performance as long as the beam shape at the isocenter remains round and consistent.

Figure 8 illustrates the scanning grids of the beam spots before and after the compensation at three momentum offsets of $\Delta p/p = -9.5\%$, 0%, and 10.5%. The gray dashed boxes in the figure represent the regions in which all the scanning points share the same NC quadrupole field setting. Owing to the symmetry of the beam transportation, the number of compensation regions is halved. The regions symmetrical to the horizontal axis share the same field settings, with only the skewed quadrupole field having the opposite sign. For a beam with a momentum offset, the situation is more complicated because the trajectory of the beam changes with the quadrupole field. Therefore, extra attention should be paid to the beam envelope when the momentum offset is large, in case it exceeds the GFR.

The beam spots in Fig. 8 are not perfectly round after compensation in the optics simulation. This problem can be addressed by a matter-particle interaction occurs when the beam passes through the nozzle, which normally leads to an increase in the size of the beam spot and turns the beam shape into a Gaussian distribution. To evaluate the beam shape including the scattering effect, a Monte Carlo simulation was conducted using TOPAS [30]. Figure 9 shows the scanning grid results after compensation at beam energies of 200 MeV and 70 MeV without momentum offset. The distortion of the beam shape is significantly reduced, particularly for the beam with an energy of 70 MeV, which has

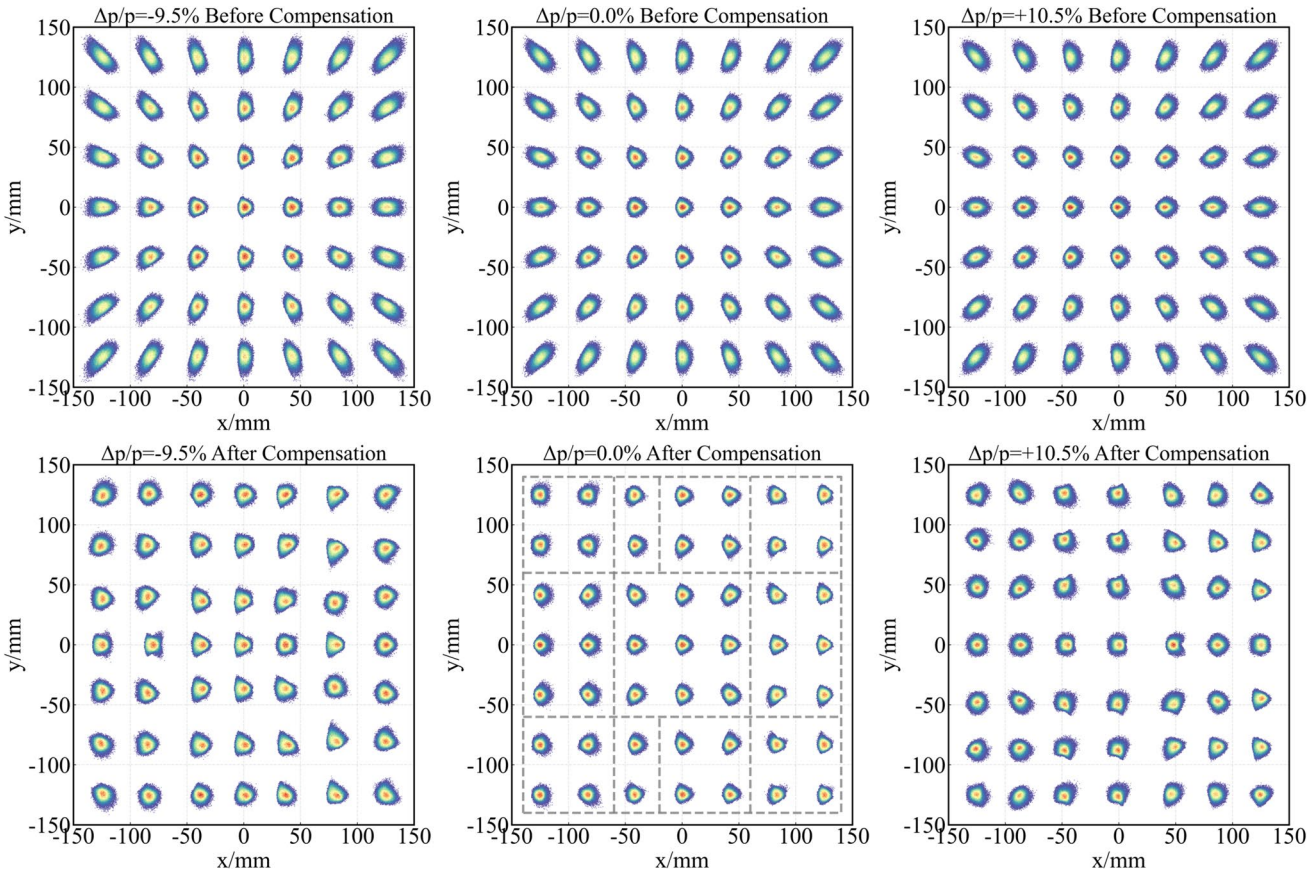

Fig. 8 (Color online) Grid scanning results before and after the compensation at three momentum offset points

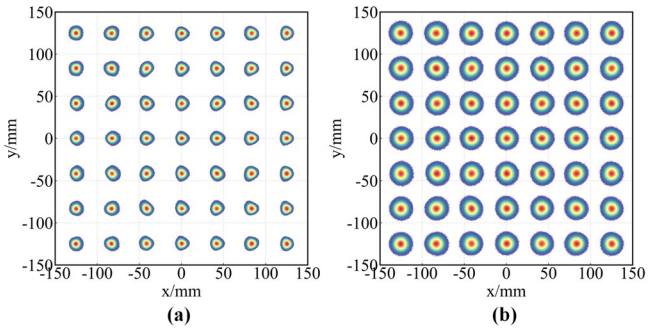

Fig. 9 (Color online) Grid scanning results with scattering effect included. **a** At a beam energy of 200 MeV. **b** At a beam energy of 70 MeV

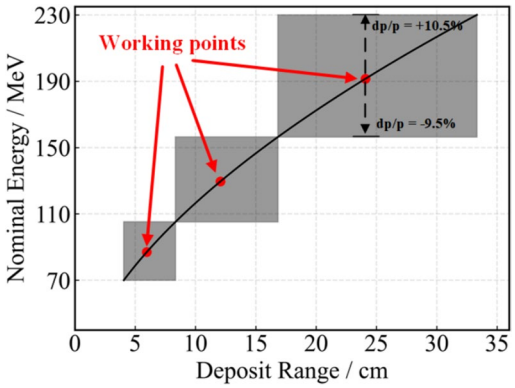

Fig. 10 (Color online) Three working points with 20% momentum acceptance to cover the dose deposition range of 4–30 cm

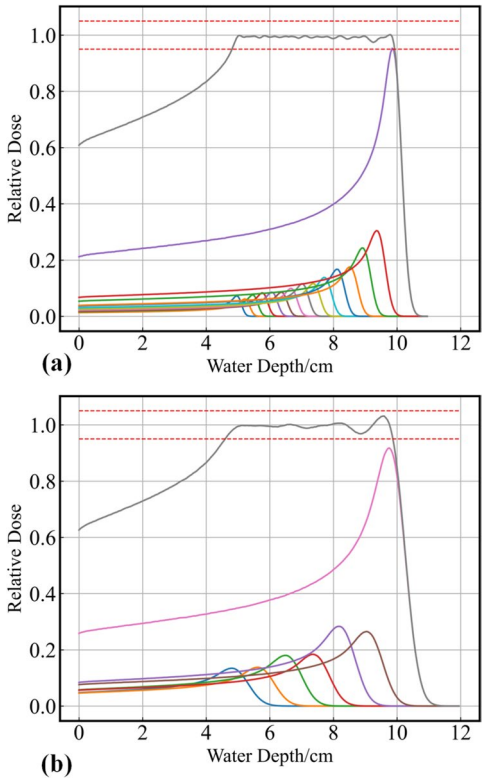

Fig. 11 (Color online) Dose deposition in water for an SOBP configuration to cover a range of 5–10 cm. **a** Beams with a fixed momentum spread of ±0.5%. **b** Beams from the LMA gantry. The red dashed lines represent the ±5% fluctuation limit of the relative dose

a positive impact on the treatment quality. For example, the ellipticity of one beam spot can be reduced from 13.25% in the optics simulation to 9.87% at 200 MeV and 3.96% at 70 MeV. The beam size barely increases at an energy of 200 MeV but dramatically increases at 70 MeV. Therefore, more attention should be given to low-beam-energy situations to prevent the beam size from exceeding this constraint. Considering the scattering effect, the constraints, as listed in Table 4, should be revised in the optical (vacuum) design. The maximum beam size should be limited to 3.8 mm (1σ) and the beam ellipticity should be relaxed to 15%.

Furthermore, by expanding the utility of tunable NC quadrupoles, ellipticity may no longer be a restriction for momentum acceptance because the beam size in both planes can be easily controlled by changing the focusing force. In other words, the bore apertures of the magnets limit the momentum acceptance range of the LMA gantry.

5 Clinical advantages of the LMA gantry

With a large momentum acceptance of 20%, the magnets on the gantry can cover the full energy range with only three working points, as shown in Fig. 10. The three points cover the deposition ranges of 4.3 cm, 8.5 cm, and 16.5 cm, respectively, such that most of the treatment can be performed without changing the fields of the AG-CCT magnets [31]. Treatment complexities can be reduced because AC losses, hysteresis effects, field checks, and field instability due to the magnet ramp affect the efficacy and efficiency of the treatment.

Combined with the use of linear motors for the degrader set, whose energy-switch duration is expected to be within 50 ms per step [32], ultrafast energy modulation can be achieved. This can be advantageous for volumetric

repainting, beam-tracking technology, and proton arc therapy [33].

In addition, a high-intensity beam with a large energy spread is another attractive advantage of the LMA gantry benefitting from an untruncated beam, which could help increase treatment efficiency by reducing the beam delivery time and number of energy layers. Therefore, patient throughput can be increased [34–37]. In Fig. 11, we compare the Spread-Out Bragg Peak (SOBP) configuration between the conventional small-momentum-spread beam and the beam from the LMA gantry to cover a water depth ranging from 5 to 10 cm, which both meet the clinical requirement of the ±5% fluctuation limit. Beams with a fixed momentum spread of ±0.5% require 15 layers of energy stacking to realize a uniform SOBP, whereas the LMA beams require only seven layers. The pitches of the energy layers were determined from the widths of the Bragg peaks. With a broader Bragg peak width, the irradiation time is effectively shortened, and the beams become more robust to position uncertainties [38]. However, the distal penumbra is also broadened because of wide Bragg peaks, which can increase the dose to the organs at risk. To mitigate this, the optimization of spot weights using IMPT [39] may be a solution. A conformal dose could be achieved by decreasing the weight of the periphery and rearranging the interior spots. In addition, utilizing small spots at the target periphery and large spots in the center, known as the mixed-size spot-scanning method [40], can be conducive to both penumbra reduction and fast treatment.

6 Conclusions and outlook

In this study, a compact LMA gantry based on AG-CCT magnets was proposed. The gantry adopts a hybrid SC design with a high-transmission degrader situated in the middle. The degrader modulates the beam energy in a stepwise manner with hybrid materials, which provides both low-emittance growth and a short energy switch time. AG-CCT magnets were introduced into the SC section as effective achromatic elements, whose magnetic fields are symmetrically set. Its combined-function field can reduce the number of magnets in the gantry and enrich the design flexibility. An optics simulation proved that the gantry could transport the beam with a momentum acceptance of approximately 20%. Treatments can be performed with a few switches of the SC magnetic fields. Rapid dose delivery can be achieved. Proton beams with full energy spread can pass to the isocenter without truncating the energy spectrum, which can significantly increase the dose rate but also cause severe dispersion effects. Therefore, a compensation method was proposed. By tuning the magnetic field of the quadrupoles corresponding to the scanning points, a beam with a maximum energy spread of ±5.2% can be delivered to the target volume with a high-quality shape. The tunable NC quadrupole can also provide redundant regulation during treatment to ensure the stability of the beam optics. In summary, the LMA gantry designed in this study has good feasibility. Its compact layout and high treatment efficiency may be beneficial for patients and hospitals.

In the next stage, detailed designs of the magnets will be performed, especially the AG-CCT magnets. However, problems remain in the development and fabrication of AG-CCTs. A curved AG-CCT magnet with a large bore would catalyze the field distortion. For example, the magnetic center deviates from the geometric center. Unexpected fields in the combined-function magnet can affect the beam transportation. In addition, the relationship between the winding path and transverse field of the AG-CCT cannot be characterized in a precise and practical way. We attempted to develop an AG-CCT design framework that includes winding path design, harmonic suppression, and fringe field optimization. Subsequently, multiparticle tracking was performed based on a realistic field distribution to validate the lattice design. Error analysis of the gantry beamline to test the robustness of the lattice is ongoing.

Author contributions All authors contributed to the study conception and design. Directional guidance was provided by Bin Qin and Xu Liu. Material preparation, data collection and analysis were performed by Wei Wang, Zi-Yi Yang and Qu-Shan Chen. The first draft of the manuscript was written by Yi-Cheng Liao and all authors commented on previous versions of the manuscript. All authors read and approved the final manuscript.

Declarations

Conflict of interest The authors declare that they have no conflict of interest.

References

1. E. Pedroni, R. Bearpark, T. Böhringer et al., The PSI Gantry 2: a second generation proton scanning gantry. Z. Med. Phys. **14**, 25–34 (2004). https://doi.org/10.1078/0939-3889-00194
2. E. Pearson, O. de Wilde, R. Doyen et al., Magnet developments and commissioning for the IBA compact gantry. IEEE Trans. Appl. Supercond. **24**, 1–4 (2014). https://doi.org/10.1109/TASC.2013.2284719
3. A. Gerbershagen, C. Calzolaio, D. Meer et al., The advantages and challenges of superconducting magnets in particle therapy. Supercond. Sci. Technol. **29**, 083001 (2016). https://doi.org/10.1088/0953-2048/29/8/083001
4. J. Flanz, H. Owen, M. Schippers, Report on Workshop: Modern Hadron Therapy Gantry Developments. CERN-ACC-NOTE (2014). http://cds.cern.ch/record/1965991. Accessed 10 Mar 2014
5. A. Gerbershagen, D. Meer, J.M. Schipers et al., A novel beam optics concept in a particle therapy gantry utilizing the advantages of superconducting magnets. Z. Med. Phys. **26**, 224–237 (2016). https://doi.org/10.1016/j.zemedi.2016.03.006

6. W.S. Wan, L. Brouwer, S. Caspi et al., Alternating-gradient canted cosine theta superconducting magnets for future compact proton gantries. Phys. Rev. ST Accel. Beams **18**, 103501 (2015). https://doi.org/10.1103/PhysRevSTAB.18.103501
7. L.N. Brouwer, *Dissertation* (University of California, Berkeley, 2015)
8. K.P. Nesteruk, C. Calzolaio, M. Seidel et al., Beam optics of a superconducting proton therapy gantry with a large momentum acceptance. Int. J. Mod. Phys. A **34**, 1942024 (2019). https://doi.org/10.1142/S0217751X19420247
9. M. Han, J. Zheng, Y. Cheng et al., Optical design and higher-order aberrations with the superconducting gantry based on limited ramping fields. Nucl. Instrum. Methods Phys. Res. A **1049**, 168086 (2023). https://doi.org/10.1016/j.nima.2023.168086
10. L. Brouwer, A. Huggins, W.S. Wan, An achromatic gantry for proton therapy with fixed-field superconducting magnets. Int. J. Mod. Phys. A **34**, 1942023 (2019). https://doi.org/10.1142/S0217751X19420235
11. L. Botuura, E. Felcini, G. de Rijk et al., GaToroid: a novel toroidal gantry for hadron therapy. Nucl. Instrum. Methods Phys. Res. A **983**, 164588 (2020). https://doi.org/10.1016/j.nima.2020.164588
12. K.P. Nesteruk, A. Bolsi, A.J. Lomax et al., A static beam delivery device for fast scanning proton arc-therapy. Phys. Med. Biol. **66**, 055018 (2021). https://doi.org/10.1088/1361-6560/abe02b
13. Y.Q. Yang, W.C. Fang, X.X. Huang et al., Static superconducting gantry based proton CT combined with X ray CT as prior image for FLASH proton therapy. Nucl. Sci. Tech. **34**, 11 (2023). https://doi.org/10.1007/s41365-022-01163-2
14. B. Qin, X. Liu, Q.S. Chen et al., Design and development of the beamline for a proton therapy system. Nucl. Sci. Tech. **32**, 138 (2021). https://doi.org/10.1007/s41365-021-00975-y
15. Y.C. Liao, R.X. Zhao, X. Liu et al., High order beam optics optimization for a superconducting gantry applied to proton therapy based on NSGA-III. Nucl. Instrum. Methods Phys. Res. A **1014**, 165727 (2021). https://doi.org/10.1016/j.nima.2021.165727
16. R.X. Zhao, B. Qin, Y.C. Liao et al., Achieving a realistic design for a superconducting gantry with large momentum acceptance for proton therapy. Nucl. Instrum. Methods Phys. Res. A **1015**, 165773 (2021). https://doi.org/10.1016/j.nima.2021.165773
17. J. Heese, J. Wulff, A. Winnerbeck, A. Huggins, M. Schillo, Clinical aspects of compact gantry design, in *Workshop of Superconductivity and other new Developments in Gantry Design for Particle Therapy, in Superconductivity and other new Developments in Gantry Design for Particle Therapy*, Bad Zurzach, Switzerland, 17–19 Sept (2015). https://indico.psi.ch/event/3575/contributions/6949/attachments/6130/7758/05_J_Heese.pdf
18. K. Makino, M. Berz, COSY INFINITY version 9. Nucl. Instrum. Methods Phys. Res. A **558**, 346–350 (2006). https://doi.org/10.1016/j.nima.2005.11.109
19. F. Jiang, K.Z. Ding, G. Chen et al., Design study of a compact superconducting cyclotron SC240 for proton therapy. in *Proceedings of the 10th International Accelerator Conference*, Melbourne, Australia, 19–24 May (2019). https://doi.org/10.18429/JACoW-IPAC2019-THPMP029
20. Z.K. Liang, K.F. Liu, B. Qin et al., Design and optimization of an energy degrader with a multi-wedge scheme based on Geant4. Nucl. Instrum. Methods Phys. Res. A **890**, 112–118 (2018). https://doi.org/10.1016/j.nima.2018.01.073
21. X. Liu, W. Wang, Z.K. Liang et al., Design of a light and fast energy degrader for a compact superconducting gantry with large momentum acceptance. Physica Med. **73**, 43–47 (2020). https://doi.org/10.1016/j.ejmp.2020.04.008
22. A.M. Huggins, *Novel Beam Optics of Achromatic Superconducting Gantries for Proton Therapy* (AUS Columbia, South Carolina, 2020)
23. S. Agostinelli, J. Allison, K. Amako et al., Geant4—a simulation toolkit. Nucl. Instrum. Methods Phys. Res. A **506**, 250–303 (2003). https://doi.org/10.1016/S0168-9002(03)01368-8
24. C.C. Chen, C. Chang, M.F. Moyers et al., Technical Note: Spot characteristic stability for proton pencil beam scanning. Med. Phys. **43**, 777–782 (2016). https://doi.org/10.1118/1.4939663
25. E. Pedroni, D. Meer, C. Bula et al., Pencil beam characteristics of the next-generation proton scanning gantry of PSI: design issues and initial commissioning results. Eur. Phys. J. Plus **126**, 66 (2011). https://doi.org/10.1140/epjp/i2011-11066-0
26. U.W. Langner, J.G. Eley, L. Dong et al., Comparison of multi-institutional Varian ProBeam pencil beam scanning proton beam commissioning data. J. Appl. Clin. Med. Phys. **18**, 96–107 (2017). https://doi.org/10.1002/acm2.12078
27. M. Li, J.X. Zheng, Y.T. Song et al., Beam optics and isocenter property of SC200 proton therapy gantry. Nucl. Sci. Tech. **29**, 112 (2018). https://doi.org/10.1007/s41365-018-0446-5
28. K. Deb, H. Jain, An evolutionary many-objective optimization algorithm using reference-point-based nondominated sorting approach, part I: solving problems with box constraints. IEEE Trans. Evolut. Comput. **18**, 577–601 (2014). https://doi.org/10.1109/TEVC.2013.2281535
29. W. Wang, X. Liu, Z.Y. Yang et al., Improving delivery efficiency using spots and energy layers reduction algorithms based on a large momentum acceptance beamline. Med. Phys. **50**, 5189–5200 (2023). https://doi.org/10.1002/mp.16420
30. J. Perl, J. Shin, J. Schümann et al., TOPAS: an innovative proton Monte Carlo platform for research and clinical applications. Med. Phys. **39**, 6818–6837 (2012). https://doi.org/10.1118/1.4758060
31. K. Suzuki, M.T. Gillin, N. Sahoo et al., Quantitative analysis of beam delivery parameters and treatment process time for proton beam therapy. Med. Phys. **38**, 4329–4337 (2011). https://doi.org/10.1118/1.3604153
32. A.C. Giovannelli, V. Maradia, D. Meer et al., Beam properties within the momentum acceptance of a clinical gantry beamline for proton therapy. Med. Phys. **49**, 1417–1431 (2022). https://doi.org/10.1002/mp.15449
33. G. Fattori, Y. Zhang, D. Meer et al., The potential of Gantry beamline large momentum acceptance for real time tumour tracking in pencil beam scanning proton therapy. Sci. Rep. **10**, 15325 (2020). https://doi.org/10.1038/s41598-020-71821-1
34. V. Maradia, D. Meer, D.C. Weber et al., A new emittance selection system to maximize beam transmission for low-energy beams in cyclotron-based proton therapy facilities with gantry. Med. Phys. **48**, 7613–7622 (2021). https://doi.org/10.1002/mp.15278
35. V. Maradia, A.C. Giovannelli, D. Meer et al., Increase of the transmission and emittance acceptance through a cyclotron-based proton therapy gantry. Med. Phys. **49**, 2183–2192 (2022). https://doi.org/10.1002/mp.15505
36. V. Maradia, D. Meer, R. Dölling et al., Demonstration of momentum cooling to enhance the potential of cancer treatment with proton therapy. Nat. Phys. **19**, 1437–1444 (2023). https://doi.org/10.1038/s41567-023-02115-2
37. J.Y. Liu, X. Yu, C. Wu et al., Design of an ultra-high dose rate cell irradiation experimental platform using a medical proton linear injector. Nucl. Tech. (in Chinese) **46**, 110201 (2023). https://doi.org/10.11889/j.0253-3219.2023.hjs.46.110201
38. S. Fujitaka, T. Takayanagi, R. Fujimoto et al., Reduction of the number of stacking layers in proton uniform scanning. Phys. Med. Biol. **54**, 3101–3111 (2009). https://doi.org/10.1088/0031-9155/54/10/009
39. X. Zhang, Y. Li, X. Pan et al., Intensity-modulated proton therapy reduces the dose to normal tissue compared with intensity-modulated radiation therapy or passive scattering proton therapy and enables individualized radical radiotherapy for extensive stage IIIB non-small-cell lung cancer: a virtual clinical study. Int. J. Radiat.

Oncol. Biol. Phys. **77**, 357–366 (2010). https://doi.org/10.1016/j.ijrobp.2009.04.028

40. Y.L. Yan, X.G. Liu, Z.Y. Dai et al., Spot-scanning beam delivery with laterally- and longitudinally-mixed spot size pencil beams in heavy ion radiotherapy. Chin. Phys. C **41**, 098201 (2017). https://doi.org/10.1088/1674-1137/41/9/098201